Palaeogeography, Palaeoclimatology, Palaeoecology 435 (2015) 38–52

Contents lists available at ScienceDirect

Palaeogeography, Palaeoclimatology, Palaeoecology

journal homepage: www.elsevier.com/locate/palaeo

Lilliput effect in freshwater ostracods during the Permian–Triassic extinction

Daoliang Chu [a], Jinnan Tong [a,*], Haijun Song [a], Michael J. Benton [b], Huyue Song [a], Jianxin Yu [a], Xincheng Qiu [a], Yunfei Huang [a,c], Li Tian [a]

[a] State Key Laboratory of Biogeology and Environmental Geology, School of Earth Sciences, China University of Geosciences, Wuhan 430074, China
[b] School of Earth Sciences, University of Bristol, Bristol, BS8 1RJ, UK
[c] School of Geosciences, Yangtze University, Wuhan 430010, China

ARTICLE INFO

Article history:
Received 14 February 2015
Received in revised form 27 May 2015
Accepted 3 June 2015
Available online 11 June 2015

Keywords:
Permian–Triassic transition
Lilliput effect
Extinction
Ostracod
Terrestrial
Freshwater

ABSTRACT

The Lilliput effect following the Permian–Triassic mass extinction and its aftermath has been documented in a variety of marine animal groups, but it is less known in terrestrial and freshwater invertebrates. Here we present new investigations of the size variations of terrestrial ostracods of the genus *Darwinula* based on fossil records from a Permian–Triassic section on the northern limb of the Dalongkou Anticline section in Northwest China. Quantitative analyses reveal that ostracod test sizes decreased sharply through the terrestrial Permian–Triassic mass extinction interval. The Lilliput effect in terrestrial ostracods is characterized by the extinction of large taxa and the rise of small-sized and elongate new forms, coupled with the dramatic loss of conchostracans, charophytes, and the blooming of lycopod spores. The size decrease in terrestrial ostracods, following the biotic crisis through the Permian–Triassic interval, was probably triggered by several interacting events, including global warming, anoxia, and enhanced sediment input following acid rain and wildfire.

1. Introduction

The Permian–Triassic (P–Tr) biotic crisis, as the greatest such event in the Phanerozoic, eliminated more than 90% of marine species and up to 70% of terrestrial vertebrate species (Erwin, 1993; Benton, 2003; Song et al., 2013). It is likely that the collapse of terrestrial ecosystems was simultaneous with the marine mass extinction during the P–Tr transitional time (Twitchett et al., 2001; S.Z. Shen et al., 2011; Metcalfe et al., 2015). A large amount of evidence of global warming, anoxia, ocean acidification, wildfire, enhanced terrestrial weathering, and other environmental factors have been proposed as responsible for the extreme and unusual conditions during the P–Tr crisis (Wignall and Twitchett, 1996; Isozaki, 1997; Algeo and Twitchett, 2010; Algeo et al., 2011; Clapham and Payne, 2011; S.Z. Shen et al., 2011; W.J. Shen et al., 2011; Hinojosa et al., 2012; Joachimski et al., 2012; Sedlacek et al., 2014). Recent studies demonstrate that these terrible environmental conditions were not only prevalent during the P–Tr crisis, but also lasted throughout most of the Early Triassic (Song et al., 2012; Sun et al., 2012; Grasby et al., 2013; Tian et al., 2014), which resulted in a catastrophic world with low biotic diversity in the aftermath of the P–Tr extinction (Hallam and Wignall, 1997; Song et al., 2011a; Chen and Benton, 2012).

Most work on the P–Tr mass extinction has focused on marine records, but less is known about the change of ecosystems in terrestrial facies. In fact, abnormal climatic conditions observed from marine records, such as global warming, wildfire, and enhanced weathering, would have had a severe impact on the terrestrial ecosystem and synchronously caused great losses of vertebrates and plants (Benton, 1985; Retallack et al., 1996, 2011; Retallack et al., 2003; Benton et al., 2004; Retallack, 2013; Benton and Newell, 2014; Yu et al., 2015). Widespread braided river systems are believed to have resulted from the combination of the decreased vegetation coverage and enhanced terrestrial weathering (Newell et al., 1999; Ward et al., 2000).

The aftermaths of mass extinctions are often characterized by evidence of distinct changes in intrinsic factors of fossil records. Across the P–Tr extinction horizon, the "Lilliput effect" (Urbanek, 1993; Twitchett, 2007) has been documented in many marine organisms, including foraminifers, gastropods, bivalves, brachiopods, echinoderms, and fishes (Hayami, 1997; Fraiser and Bottjer, 2004; Chen et al., 2005; Payne, 2005; Twitchett et al., 2005; He et al., 2007, 2010; Twitchett, 2007; McGowan et al., 2009; Mutter and Neuman, 2009; Song et al., 2011b; He et al., 2015; Romano et al., 2015). For land organisms, the P–Tr extinction is associated with evidence of temporary body size reductions in terrestrial vertebrates and

* Corresponding author at: State Key Laboratory of Biogeology and Environmental Geology, School of Earth Sciences, China University of Geosciences, Wuhan, 430074, China. Tel.: +86 27 67883450.
E-mail address: jntong@cug.edu.cn (J. Tong).

http://dx.doi.org/10.1016/j.palaeo.2015.06.003
0031-0182/

freshwater bony fishes (Tverdokhlebov et al., 2002; Huttenlocker, 2014; Romano et al., 2015). However, the change of body sizes has been scarcely studied for terrestrial aquatic invertebrates during the P–Tr mass extinction. Our investigation of the size variations of terrestrial ostracods belonging to the genus *Darwinula*, which is one of the most typical invertebrates during the P–Tr transitional interval, demonstrates that the Lilliput effect did occur in terrestrial aquatic organisms following this severe event, and suggests that the fossil records from non-marine facies show a similar response to the environmental events across the P–Tr crisis as those in the marine ecosystems.

2. Stratigraphic setting and studied section

Well-exposed non-marine P–Tr transitional successions are located on the southern flank of the Junggar Basin in the foothills of the Tian Shan (Bogda Shan) Mountain, Xinjiang, Northwest China (Fig. 1). In particular, many biostratigraphic investigations have been undertaken on both south and north limbs of the Dalongkou Anticline (SLA and NLA sections), and the SLA section has been suggested as the candidate Accessary Stratotype Section and Point (ASSP) for the global non-marine P–Tr boundary (PTB) (Liu, 1994; Cheng et al., 1997; Hou, 2004; Pang and Jin, 2004; Metcalfe et al., 2009; Kozur and Weems, 2011). The first occurrence of the Early Triassic vertebrate *Lystrosaurus* has been suggested as a major marker of the terrestrial PTB, and this is located in the upper part of the Guodikeng Formation in the SLA section (Cheng et al., 1997). Based on palynological data from the Guodikeng Formation, Metcalfe et al. (2009) suggested that the PTB might be placed approximately 50 m below the top of the Guodikeng Formation in their measured lithostratigraphic sequence, with a distinct change in the sporomorphs at the base of Assemblage 3, i.e. the *Lundladispora foveota–Pechorasporites disertus–Otynisporites eotriassicus* assemblage. A later study indicated that an overlapping interval of sporomorphs occurs in the middle part of the Guodikeng Formation, based on the data of denser palynological samples from the SLA section (Hou, 2004); this study placed the PTB at the base of Bed 51 of the measured lithostratigraphic section, where the Mesozoic progenitors of *Lundbladispora* and *Taeniaesporites* gradually became predominant. In addition, a distinct turnover in the ostracod assemblages was observed in the Guodikeng Formation by investigating the same samples as Hou (2004). The characteristic late Permian elements such as *Panxiania*, *Darwinula parallela* and *D. elongata*, were replaced by the *Darwinula rotundata–D. gloria–D. pseudooblonga* assemblage at the horizon approximately 10 m above the PTB suggested by palynological analysis (Pang and Jin, 2004). Furthermore, the appearance of the megaspore *Otynisporites eotriassicus* within Beds 63 to 65 of the measured

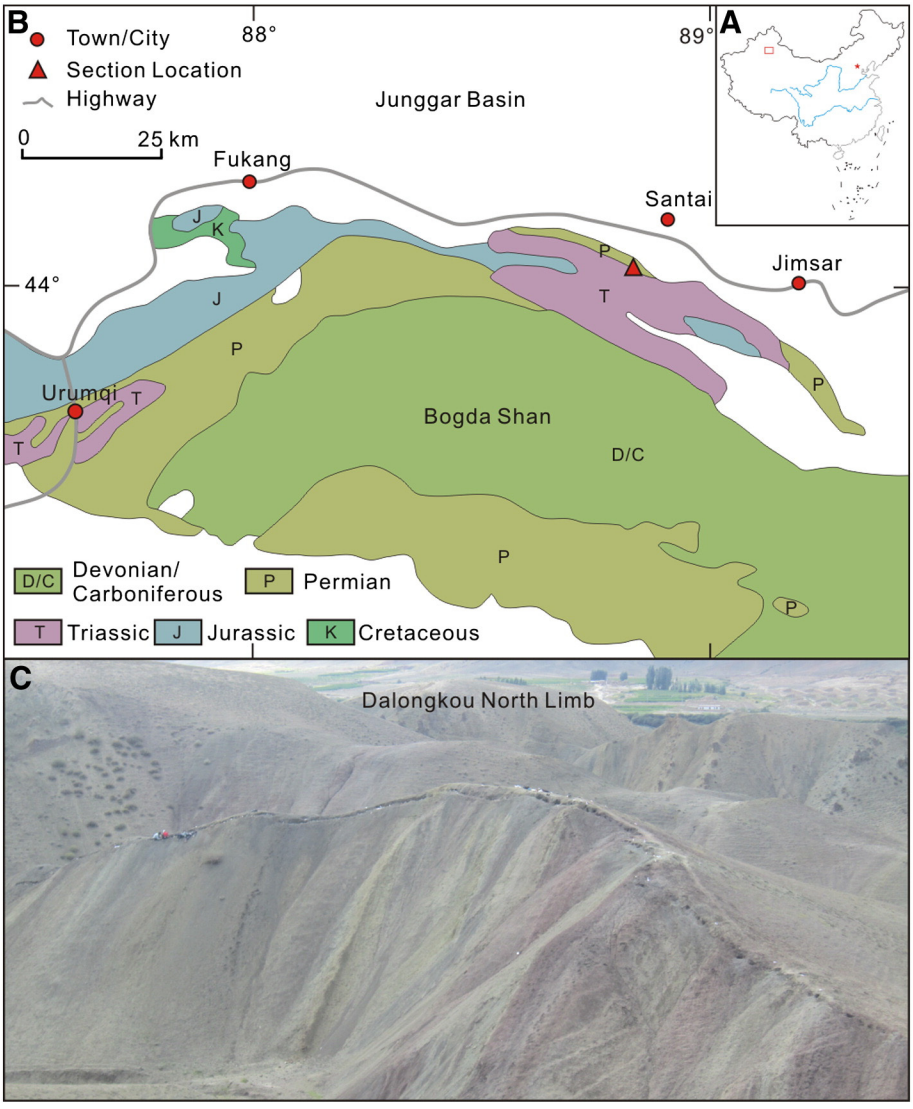

Fig. 1. Location map of the studying area and section and photograph of the outcrop. (A) Sketch map of China, the red box showing the studying area. (B) Simplified geological map of the studied area and location of the studied section, NLA section (modified from Metcalfe et al., 2009). (C) Photograph of the outcrop showing the trench on the ridge.

lithostratigraphic section of Hou (2004) marks the PTB within this interval (Foster and Afonin, 2005). Because they are common fossils in freshwater and brackish deposits, conchostracans are very important index fossils for intercontinental Triassic correlations (Kozur and Mock, 1993; Kozur and Weems, 2010). Kozur and Weems (2011) concluded that the conchostracan faunas at the SLA section can be well correlated with the conchostracan-rich beds in the Tunguska Basin and Germanic Basin according to the high-resolution conchostracans zonation, and they even attempted to correlate these with the marine conodont zonation, marking that the PTB in the upper part of the Guodikeng Formation, perhaps as high as the formational contact with the overlying Jiucaiyuan Formation.

Meanwhile, some studies have focused more on exploring changes of $\delta^{13}C_{org}$ than investigating the distinct changeover of biota near the P–Tr transition, especially in poorly preserved rocks or the strata that have discontinuous fossil records. The terrestrial PTB was defined at a sharp negative $\delta^{13}C_{org}$ shift in Australia (Morante, 1996), Antarctica (Krull and Retallack, 2000; Retallack and Krull, 2006), and the Karoo Basin (MacLeod et al., 2000; de Wit et al., 2002). Cao et al. (2008) revealed two intervals of distinctive low $\delta^{13}C_{org}$ values in the SLA section and suggested that the younger distinct negative $\delta^{13}C_{org}$ spike could be correlated to the sharp drops of $\delta^{13}C$ (carbonate carbon and organic carbon) in Bed 25 of the Meishan section. Moreover, data from the nearby Taoshuyuan section also show two distinguishable low $\delta^{13}C_{org}$ intervals, although the older one was more conspicuous.

Our studied NLA section is located 20 km west of Jimsar County (Fig. 1B). The Upper Permian to Lower Triassic terrestrial sedimentary sequence is represented by the Cangfanggou Group, composed of the Quanzijie, Wutonggou, Guodikeng, Jiucaiyuan, and Shaofanggou formations. This study focuses on the P–Tr transitional deposit within the Guodikeng Formation, which was formed in lacustrine facies in the area. The lower part of the Guodikeng Formation consists of dark-gray mudstones interbedded with siltstones and fine-grained greenish, buff and gray sandstones, and calcareous nodules, while the upper part is composed of purple mudstones with siltstones and fine-grained green and buff sandstones (Fig. 1C). Compared to the underlying Wutonggou Formation and the overlying Jiucaiyuan Formation, there is a lack of significant coarse terrigenous input to the lake during deposition of the Guodikeng Formation. The measured Guodikeng Formation at the studied section is ca. 190 m in thickness.

3. Materials and methods

Surface rocks were weathered, so trenches were dug to expose fresh rock for measurement and sampling (Fig. 1C). Sixty-eight fine-grained siliciclastic samples, each more than 150 g in weight, were collected. The hydrogen peroxide (H_2O_2)-etching method (Sohn, 1961) and a biological microscope were used to separate and select the ostracod fossils. Then, the distribution of ostracods was plotted on the stratigraphic column (Fig. 2). In addition, spores and pollen were independently considered, and a minimum of 250 spores and pollen per sample were counted for quantitative analysis. In this study, the volume (V) of the ostracod specimens was used as a major size proxy. The length (L), height (H), and thickness (T) of the tests were measured with a microscale under the microscope, and the volume (V) of each specimen was estimated based on its ellipsoid shape (Fig. 3):

$$V = \pi * L * H * T/6.$$

In this study, the test volumes were calculated by indicating the log micron cubed units to two decimal places. Only specimens of the genus *Darwinula*, which is one of the most common ostracod taxa through the terrestrial P–Tr interval, were used for the statistical study in order to avoid the possible size difference of various genera. Finally, 551 specimens of *Darwinula* were isolated from 24 samples, and measured for the analysis of body size. The mean size, distribution histogram, standard deviation and 95% confidence interval of the mean size were used to analyze the size distribution and variation of the ostracod specimens. The mean size (X) reflects the condition of a community:

$$X = 1/N * \sum_{i=1}^{N} Vi,$$

where X is the mean size, N is the number of fossils measured in each bed and Vi is the test volume in logarithmic scale. The 95% confidence interval of the mean is:

$$Y = t\alpha/2 * S/\sqrt{N},$$

where Y is the fluctuating range, $t_{\alpha/2}$ is the t-test value at $1 - \alpha$ confidence, S is the standard deviation, and N is the fossil number measured from each bed. The confidence interval is $(X - Y, X + Y)$, where X is the mean size, $X - Y$ is the lower line, and $X + Y$ is the upper line.

In addition, the non-parametric Kolmogorov–Smirnov (K–S) test was used to determine whether the sizes of ostracod populations of successive beds were significantly different from each other (Jablonski, 1996). LOWESS (locally weighted scatterplot smoothing, the best smoothing fitting method for irregularly distributed time-series data, cf. H.Y. Song et al., 2014) curves were calculated from these volume, length and height datasets, based upon the following equation:

$$Xi = \sum_{i=1}^{n}(1/(1 + ((T-Ti)/h)^2) * Xi)/\sum_{i=1}^{n}(1/(1 + ((T-Ti)/h)^2)),$$

where X_i is the volume, length or height value and T_i is the age or the position of the sample i ($i = 1$ to n, where n is the total number of samples). The smoothing parameter h is the ratio of the observed number in the local regression, and the total number of data, termed window width, ranges from 0 to 1.

4. Ostracod fauna

A total of 37 species in three genera of ostracods are identified, including *Darwinula*, *Panxiania* and *Tatariella* (Figs. 2–4). The species of *Darwinula* are the most dominant elements and can exceed 95% of specimens in most beds of the Guodikeng Formation. The ostracod faunas show a distinct turnover at Bed 24 and may be subdivided into two assemblage zones: the *Panxiania reticulata–Darwinula fragilformis–Darwinula parallela* assemblage zone and the *Darwinula gloria–Darwinula rotundata–Darwinula minuta* assemblage zone.

The *Panxiania reticulata–Darwinula fragilformis–Darwinula parallela* assemblage zone (Assemblage I) consists of 19 species in two genera (Figs. 2–4), including *Darwinula abstrusa*, *D. chramovi*, *D. elongata*, *D. fengfengensis*, *D. fragiliformis*, *D. handanensis*, *D. inassueta*, *D. inervis*, *D. lunijiaki*, *D. malachovi*, *D. nasalis*, *D. parafragiliformis*, *D. parallela*, *D. perlonga*, *D. santaiensis*, *D. suchonensis*, *D. zhichangensis*, *Panxiania reticulata*, and *P. subquadrata*. Most of the ostracods are well preserved as large forms. They are distributed through the lower part to the bottom of the upper part of the Guodikeng Formation, in the interval from Beds 2 to 24. In particular, *Panxiania* is commonly found in Upper Permian siliciclastic rocks (Wang, 1978; Pang, 1993) and consequently the lower part of the Guodikeng Formation would be of Late Permian age.

The *Darwinula gloria–Darwinula rotundata–Darwinula minuta* assemblage zone (Assemblage II) comprises 18 species in two genera (Figs. 2–4), including *Darwinula accuminata*, *D. benigna*, *D. concinna*, *D. dilecta*, *D. gloria*, *D. ingrate*, *D. laciniosa*, *D. lucida*, *D. minuta*, *D. oblongovata*, *D. pseudooblonga*, *D. pseudoobliqua*, *D. rotundata*, *D. sibirica*, *D.* sp., *D. triassiana*, *D. verdica*, and rare *Tatariella inassneta*.

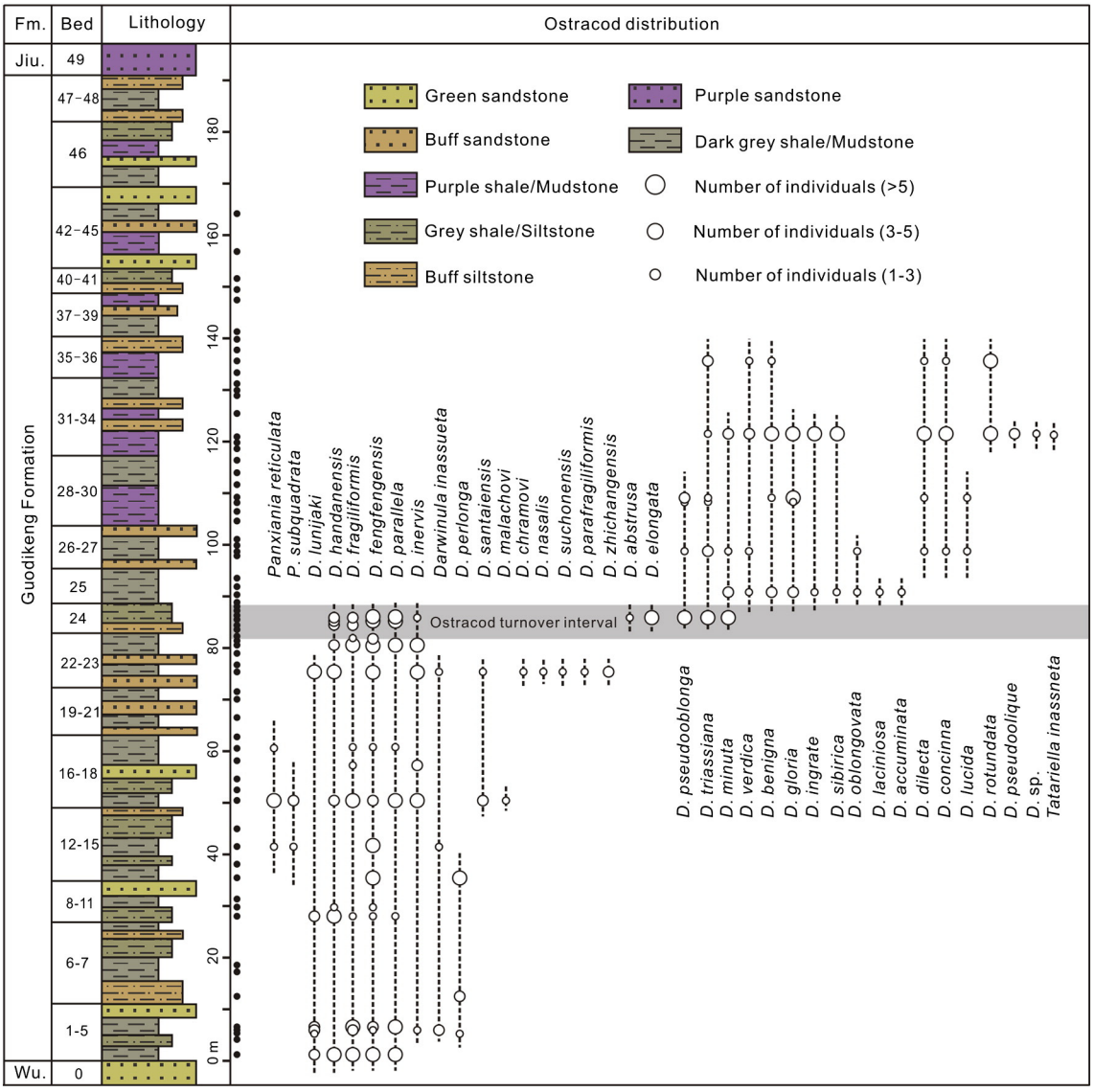

Fig. 2. The lithocolumn of the measured NLA section, showing the samples and distribution of ostracods at the section. Fm., Formation; Wu., Wutonggou Formation; Jiu., Jiucaiyuan Formation.

They are distributed in the upper part of the Guodikeng Formation (above Bed 24). The ostracod individuals have small and elongate shapes, except for a few large specimens.

5. Ostracod size variation in the studied section

The lower assemblage fossils are significantly larger than the upper forms in all measured parameters such as maximum, mean, and minimum values. The maximum test volume is up to 7.98 log μm^3, the mean test value is 7.40 log μm^3, and the minimum test value is approximately 6.56 log μm^3 from Bed 1 to Bed 23 (Table 1). The maximum, mean, and minimum test values above Bed 24 are 7.59 log μm^3, 6.93 log μm^3, and 5.87 log μm^3, respectively (Table 1). In particular, a remarkable size reduction happens in Bed 24, with maximum, mean, and minimum test values of 7.97 log μm^3, 7.11 log μm^3, and 6.15 log μm^3, respectively (Table 1). The size distributions within the two assemblages are shown in Fig. 5. The non-parametric K–S test also indicates that the most significant change ($p \ll 0.05$) in the ostracod volume of successive beds occurred between Beds 23 and 24 (Table 1).

The mean sizes of ostracod tests are relatively stable throughout the lower part of the Guodikeng Formation and fluctuate between 7.23 log μm^3 and 7.59 log μm^3. The mean sizes experience dramatic drops across the turnover horizon at the base of Bed 24. In the upper part of the Guodikeng Formation, the mean sizes remain small, between 6.70 log μm^3 and 6.97 log μm^3. In particular, ostracods with test values between 7.01 log μm^3 and 7.99 log μm^3 occur most frequently and comprise 94% of all ostracod specimens in Assemblage I of the lower part of the Guodikeng Formation (Fig. 5). In contrast, in Assemblage II of the upper part of the Guodikeng Formation, ostracods with test values between 5.01 log μm^3 and 6.99 log μm^3 are most frequent and represent 59% of all specimens (Fig. 5). Moreover, only 9% of ostracod specimens have values larger than 7.50 log μm^3 in Assemblage II, but, at least 32% of ostracod specimens reach this value in Assemblage I (Fig. 5).

Values for mean ostracod volumes and 95% confidence intervals show continuing fluctuations throughout the section (Fig. 6). There appears to be a general long-term decline in mean size from Beds 1 to 36, but there is a step between Beds 23 and 24, the only case where 95% confidence intervals do not overlap (Fig. 6A, B). The LOWESS procedure determines a best-fit trend for the changes between successive beds, and the curves indicated a significant reduction between Beds 23 and 24 (Fig. 6C). The maximum sizes of ostracod tests undergo multiple fluctuations throughout the lower part of the Guodikeng

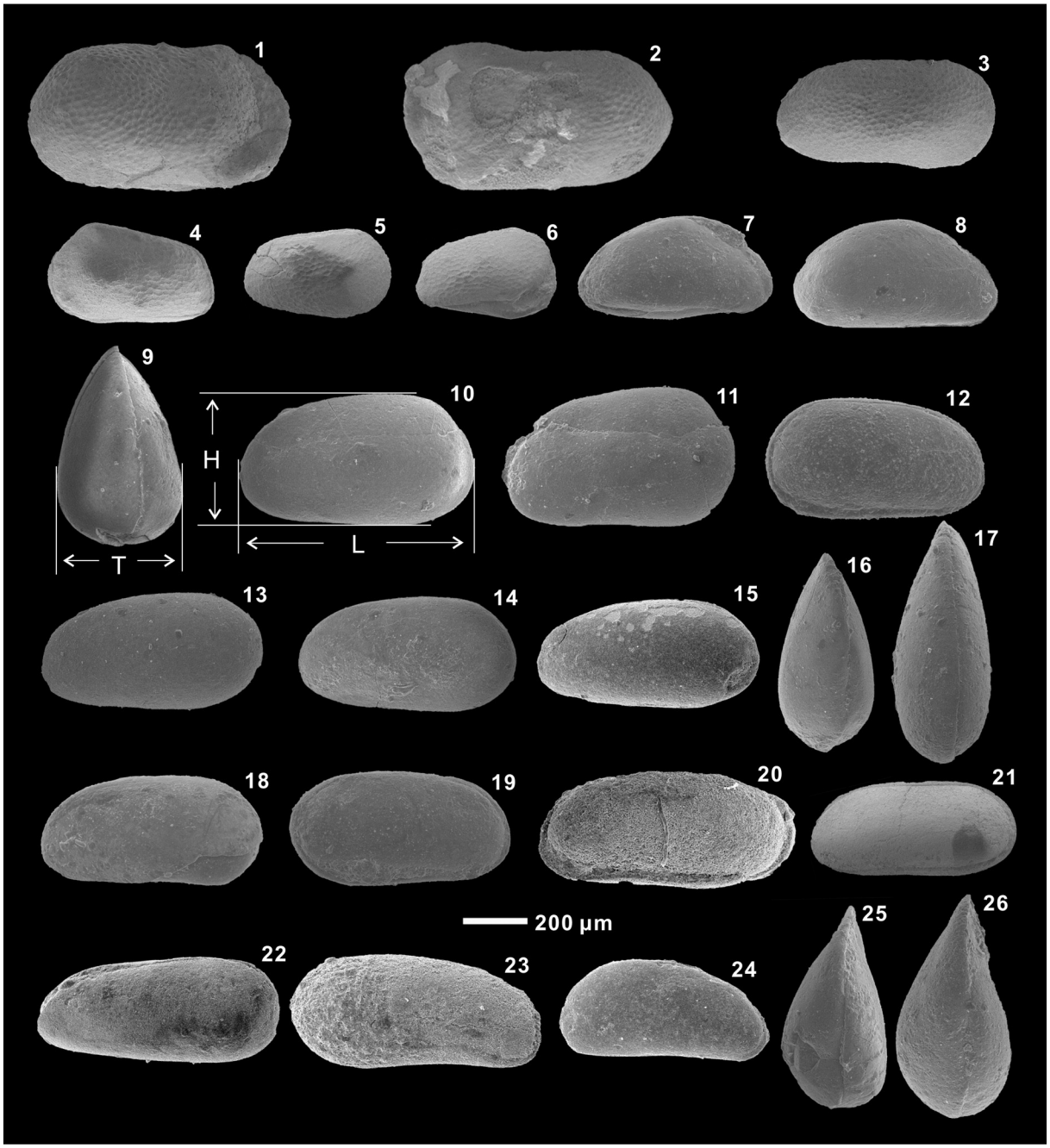

Fig. 3. Illustration of latest Permian ostracods. 1, 2. *Panxiania subquadrata*; 3. *Panxiania* sp.; 4–6. *Panxiania reticulata*; 7–9. *Darwinula fengfengensis*; 10–12. *Darwinula handensis*; 13–16. *Darwinula fragiformis*; 17–19. *Darwinula parallela*; 20, 21. *Darwinula inervis*; 22. *Darwinula chramovi*; 23. *Darwinula inassuela*; 24–26. *Darwinula lunijiaki*.

Formation, but they trend to form a plateau with maximum sizes ranging from 7.43 log μm^3 to 7.97 log μm^3 (Fig. 6). This plateau collapses and drops to a low plateau with maximum size ranging from 7.07 log μm^3 to 7.59 log μm^3 across the ostracod turnover horizon at the base of Bed 24. The most obvious difference between these two stages is the absence of the forms larger than 7.60 log μm^3 in the latter stage. The minimum sizes also follow a similar pattern to the maximum size curves in Assemblage I, ranging from 6.15 log μm^3 to 7.33 log μm^3 but with more fluctuations. The minimum size reduction was also significant because of the smaller values in the following stage that range from 5.87 log μm^3 to 6.59 log μm^3 (Fig. 6). The median value curves of ostracod tests show a similar trend in the mean value, but with greater variation, and they also experience a dramatic drop across the turnover horizon between Beds 23 and 24 (Fig. 6D).

The length, height and length to height ratio of ostracod tests also show similar changes (Fig. 7). Values for mean ostracod length and height and 95% confidence intervals show a dramatic drop during the turnover interval between Beds 23 and 24 (Fig. 7A, C). In particular, the reduction in the ostracod height data is more significant, the only transition where 95% confidence intervals do not overlap (Fig. 7C). For the Assemblage I ostracods, most individuals have length values larger than 500 μm and height values larger than 300 μm. In contrast, in Assemblage II, most individuals have length and height values ranging from 200 to 450 μm and 100 to 300 μm respectively. For instance, only

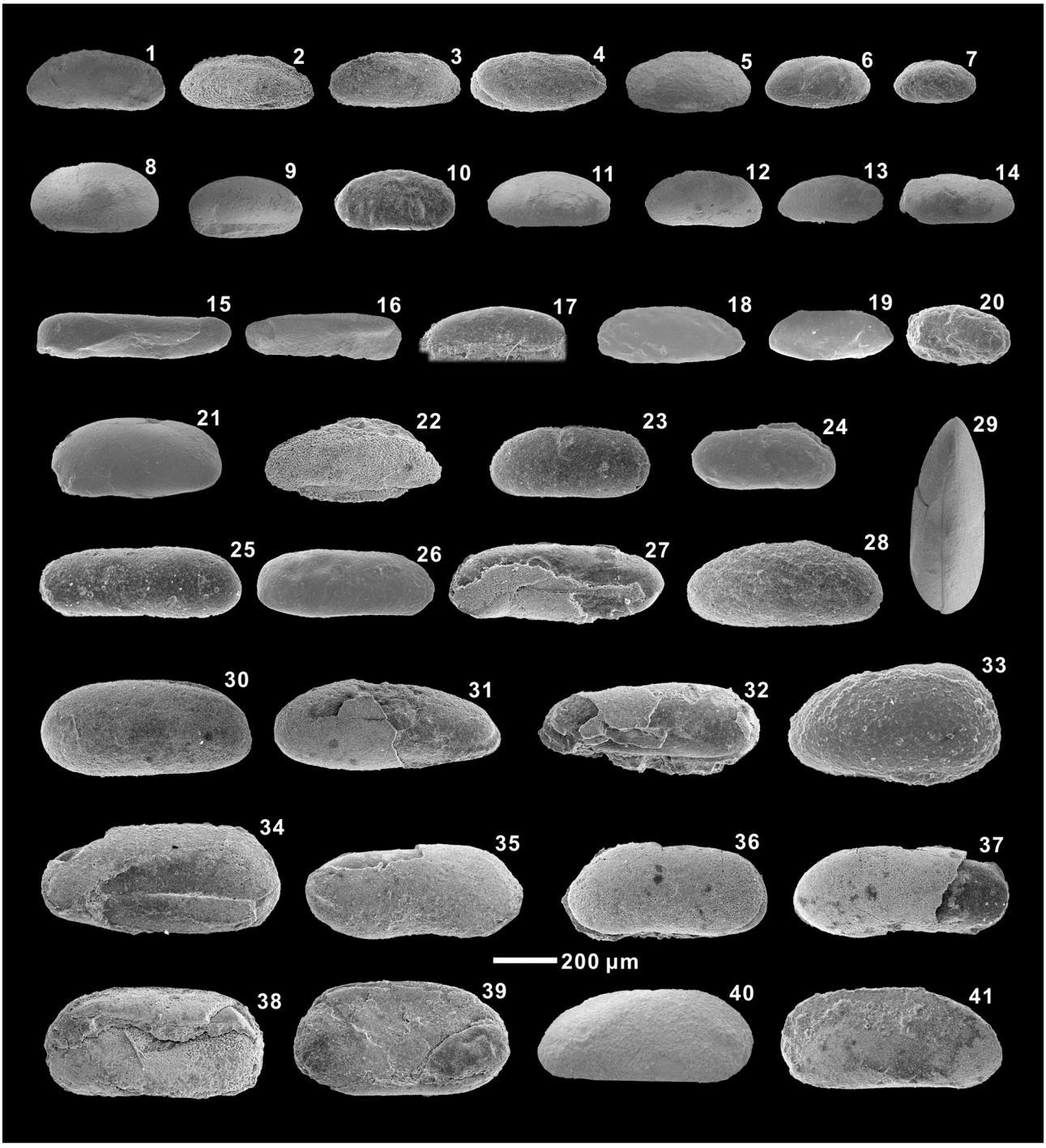

Fig. 4. Illustration of earliest Triassic ostracods. 1–3. *Darwinula ingrata*; 4. *Darwinula minor*; 5, 6. *Darwinula suchonensis*; 7. *Darwinula minuta*; 8–12. *Darwinula sibirica*; 13, 14. *Darwinula benigna*; 15, 16. *Tatariella* cf. *inassneta*; 17, 22. *Darwinula triassiana*; 18, 19. *Darwinula laciniasa*; 20. *Darwinula ovifomis*; 21. *Darwinula verdica*; 23, 24. *Darwinula pseudoobliqua*; 25–27. *Darwinula abstrusa*; 28–30. *Darwinula rotundata*; 31, 32. *Darwinula perlonga*; 33. *Darwinula accuminata*; 34. *Darwinula* cf. *fragiformis*; 35–37. *Darwinula gloria*; 38, 39. *Darwinula* cf. *parallela*; 40, 41. *Darwinula elongata*.

10% of ostracod specimens have height values larger than 350 μm in Assemblage II, but, at least 22% of ostracod specimens reach this value in Assemblage I. Moreover, the LOWESS curves indicated a significant reduction between Beds 23 and 24 both in ostracod length and height (Fig. 7B, D).

Above all, the Assemblage II ostracods are much smaller than those in Assemblage I in all measured parameters: maximum, mean, median, and minimum values of volume (Figs. 5 and 6, Table 1). The mean test volume of the lower assemblage is 7.40 log μm^3, ~3 times greater than the mean volume of the upper Assemblage II (Table 1). Analogously, the changes in length and height of ostracod tests also show significant decreases, and the Assemblage II ostracods are shorter than those in Assemblage I.

6. Discussion

6.1. The Lilliput effect following the terrestrial P–Tr crisis

A decrease of body size has been reported in the aftermath of the greatest Phanerozoic biotic crisis in a variety of animal groups (Girard

Table 1
The total number, maximum sizes, minimum sizes, mean sizes, standard deviations, 95% confidence intervals (CI) of the mean sizes, median sizes and values of Kolmogorov–Smirnov test of ostracod specimens in each bed at SLA section.

Bed number	Number of individuals	Maximum	Minimum	Mean	Standard deviation	95% CI of mean		Median	*p*-Value
1	28	7.79	7.33	7.59	0.14	7.54	7.64	7.65	N.D.
5	48	7.81	6.86	7.48	0.19	7.42	7.54	7.46	0.02027
8	18	7.80	7.21	7.53	0.17	7.45	7.61	7.57	0.30550
12	7	7.82	7.10	7.42	0.22	7.25	7.59	7.40	0.36620
15	35	7.93	6.58	7.29	0.31	7.19	7.39	7.25	0.31710
16	81	7.98	6.61	7.34	0.23	7.29	7.39	7.36	0.01264
17	7	7.43	6.96	7.23	0.18	7.09	7.37	7.22	0.19650
22	20	7.67	6.56	7.30	0.22	7.20	7.40	7.34	0.53850
23	35	7.81	6.96	7.42	0.22	7.34	7.50	7.45	0.01737
24	177	7.97	6.15	7.11	0.40	7.05	7.17	7.21	0.00000
25	12	7.36	6.59	6.92	0.23	6.79	7.05	6.92	0.01093
26	17	7.41	6.45	6.92	0.25	6.80	7.04	6.89	0.72840
29	7	7.07	6.47	6.70	0.18	6.56	6.84	6.71	0.10790
32	49	7.59	6.34	6.96	0.29	6.88	7.04	6.98	0.02910
36	10	7.33	5.87	6.97	0.42	6.70	7.24	7.12	0.32100

Footnote: *p* values show results of the Kolmogorov–Smirnov test applied to the populations of successive beds. *p* Values marked by bold font show that the populations are statistically significantly different with respect to body size at the 95% confidence level ($p < 0.05$). N.D., no data.

and Renaud, 1996; Kaljo, 1996; Renaud and Girard, 1999; Jeffery, 2001), following Urbanek (1993) who first used the term "Lilliput effect" to "describe the phenomenon of the occurrence of diminutive forms among some of the species in the relic assemblages" in the aftermaths of mass extinction events. To date, most works devoted to the study of size variation in marine organisms use the continuous and abundant fossil record, not only during the P–Tr mass extinction, but also through the entire Early Triassic (Fraiser and Bottjer, 2004; Payne, 2005; Twitchett, 2007; Song et al., 2011b). However, it was still unknown whether the Lilliput effect existed in the terrestrial aquatic invertebrates through the P–Tr events, although the phenomenon has been observed for land-based tetrapods (Tverdokhlebov et al., 2002; Huttenlocker, 2014).

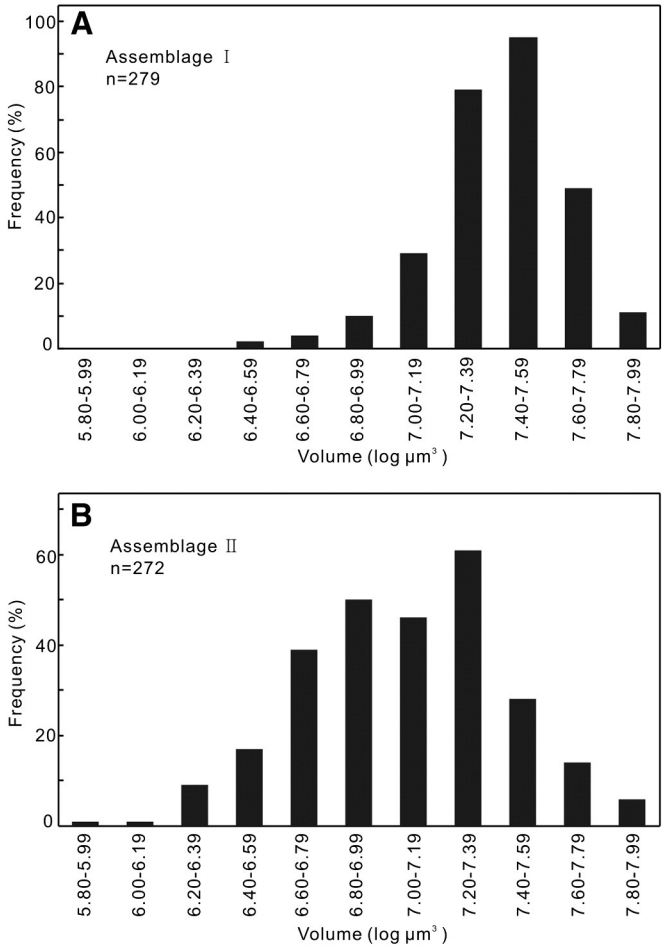

Fig. 5. Frequency of ostracod sizes (in log μm^3), both assemblages showing normal distributions. (A) Assemblage I, showing most tests are between 7.20 log μm^3 and 7.79 log μm^3 in volume, occupying 79.9% of all ostracods. (B) Assemblage II, indicating the most ostracods vary from 6.60 log μm^3 and 7.39 log μm^3 in volume, occupying 72.1% of all tests.

Our results show that a significant decline in body size of the ostracod *Darwinula* occurred in the middle part of the Guodikeng Formation in the NLA section. This evidence supports the existence of the Lilliput effect among terrestrial organisms during the P–Tr transition. Actually, Kuchtinov (1976) already reported that the large forms of *Darwinula* and *Darwinuloides* were replaced by small and elongate species of *Darwinula* and *Gerdalia* at the PTB in the Moscow Basin and suggested that the PTB could be defined at this distinct changeover, although he did not take account of a Lilliput effect related to the crisis. The appearance of the Lilliput effect could be hypothesized from this qualitative description. As for other taxa, a similar change might have occurred as a result of the same combination of intense environmental changes during the P–Tr mass extinction, although there is as yet only limited evidence.

6.2. Causes of the size reduction

6.2.1. Evolutionary patterns and size variations of various ostracod groups

Twitchett (2007) documented the Lilliput effect in animal body fossils and trace fossils during the P–Tr crisis, and proposed four possible models for the selective appearance of a shift from large to small body size, i.e. the extinction of large taxa, the appearance of small taxa, the temporary disappearance of large taxa, or within-lineage size decrease (Twitchett, 2007; Harries and Knorr, 2009). Additionally, Harries and Knorr (2009) mentioned that concerted, multidisciplinary research was required, rather than simply noting changes in size, to provide a fuller explication including all the evolutionary and ecological factors.

In our case, we see a combination of the first two models. Firstly, large species, with body sizes larger than 7.60 log μm^3, namely *Darwinula fengfengensis*, *D. fragiliformis*, *D. handensis*, *D. lunijaki*, *D. parallela*, and *D. santaiensis*, went extinct at the turnover event. In addition, specimens of *Panxiania* (no statistics) with body sizes up to 8.20 log μm^3 (Fig. 3) also disappeared above the extinction horizon.

Secondly, new forms originated immediately after the extinction event, and these were mostly smaller than the pre-extinction forms. These include *Darwinula minuta*, *D. gloria*, *D. rotundata* and *D. pseudoobliqua*, and the percentage with a body size less than 7.30 log μm^3 is up to 91% and the maximum volume is <7.60 log μm^3. It is interesting to note that the mean size value in Bed 24 is clearly

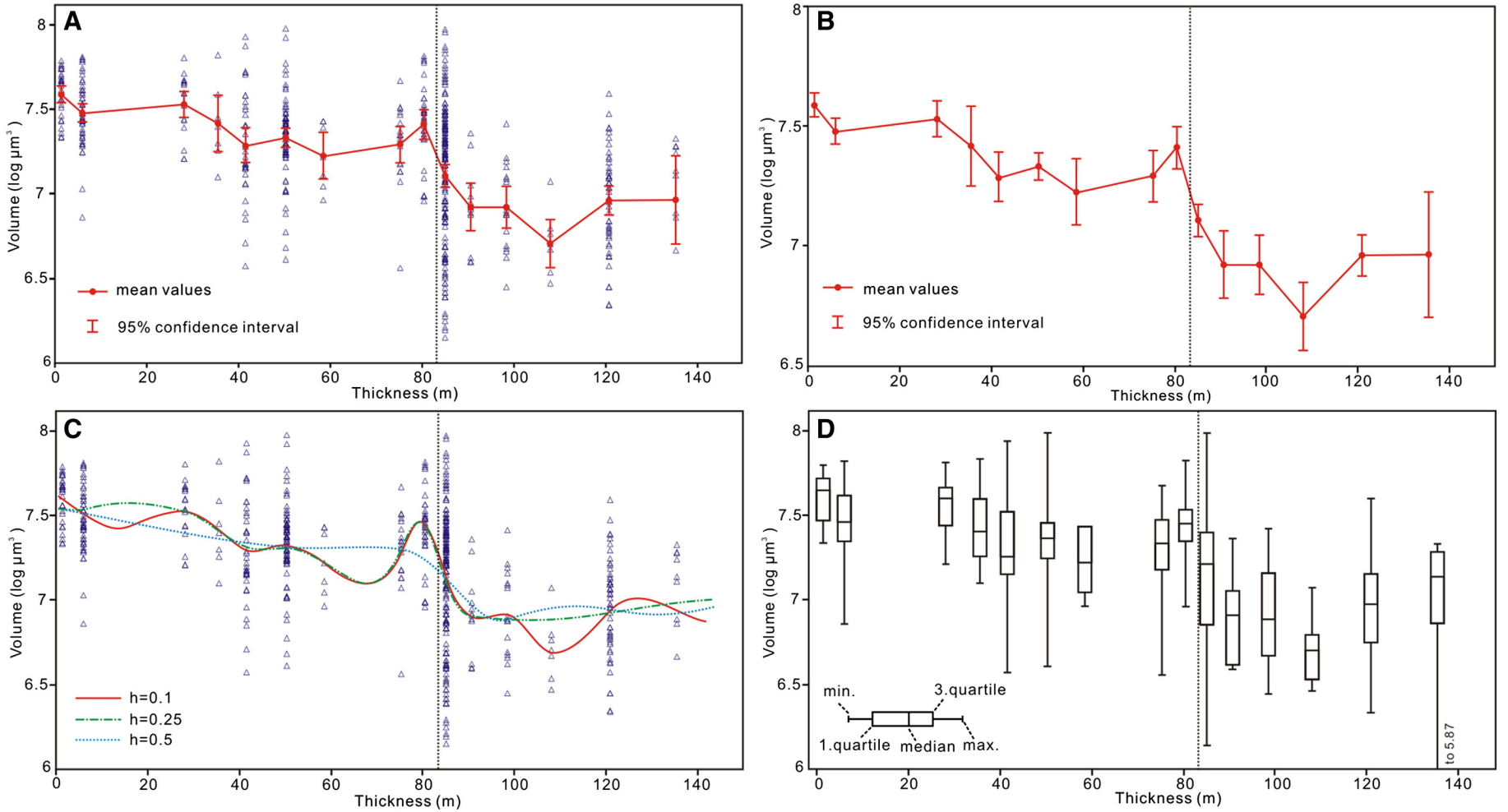

Fig. 6. Size distributions (in log µm^3) of ostracod tests through Guodikeng Formation in the NLA section. (A) Plot detail and variations in mean volume values with 95% confidence intervals for each bed, showing a significant decrease at Bed 24. (B) Variation of mean values with 95% confidence interval for each bed separately. (C) LOWESS curves from the ostracod volume dataset, with *h* (window width) set at 0.1, 0.25 and 0.5. (D) Box and whisker plots of the studied beds yielding ostracods. The dashed vertical lines represent the boundary between Beds 23 and 24.

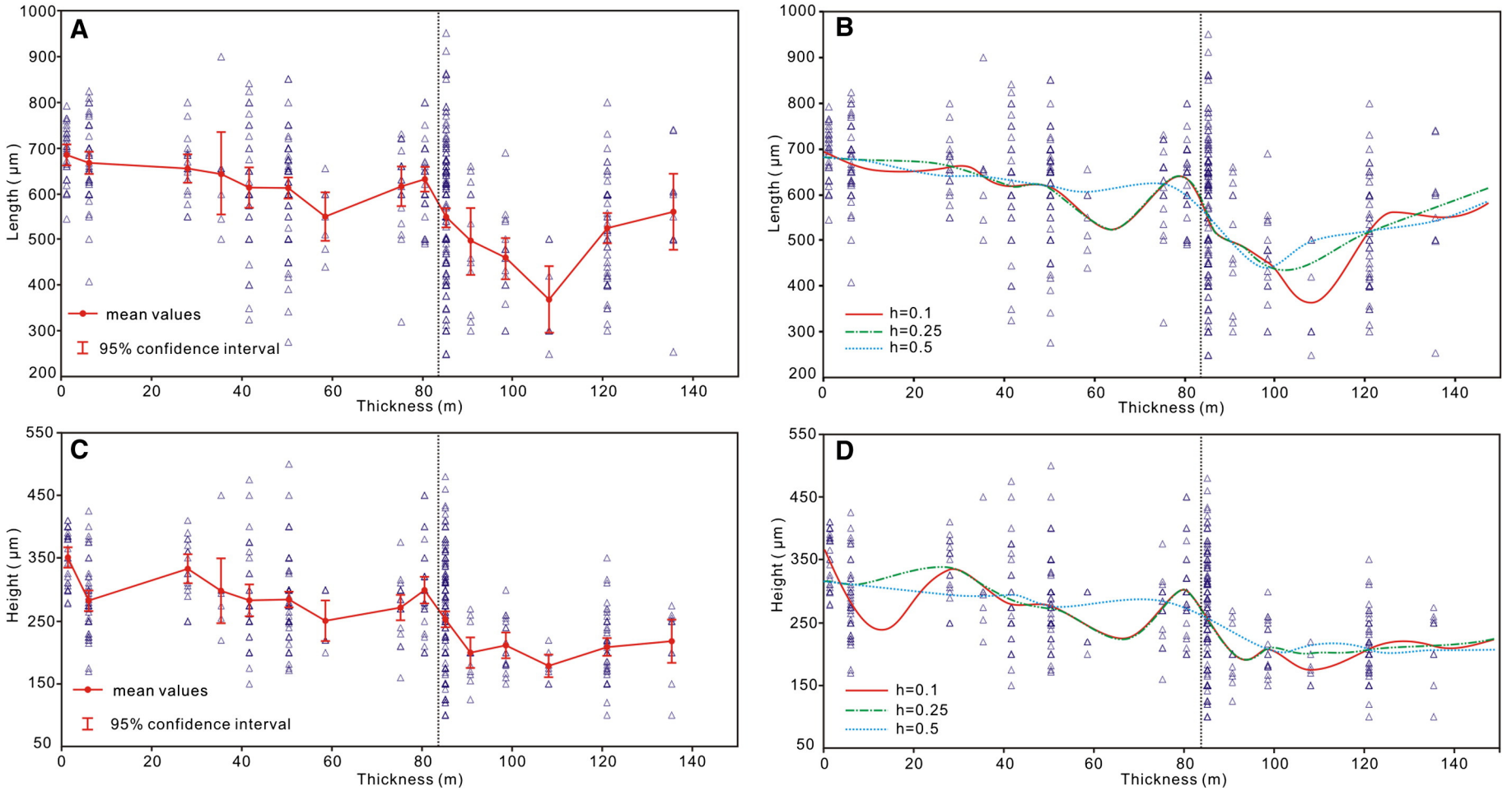

Fig. 7. Length and height distributions (in μm) of ostracod tests through Guodikeng Formation in the NLA section. (A) Plot detail and variations in mean length values with 95% confidence intervals for each bed. (B) LOWESS curves from the ostracod length dataset, with *h* (window width) set at 0.1, 0.25 and 0.5. (C) Plot detail and variations in mean height values with 95% confidence intervals for each bed. (D) LOWESS curves from the ostracod height dataset, with *h* (window width) set at 0.1, 0.25 and 0.5. The dashed vertical lines represent the boundary between Beds 23 and 24.

smaller than those from the lower strata, but larger than the specimens in the strata above. This was a result of smaller new forms originating and occupying the dominant positions. The subsequent and significant size reduction between Beds 24 and 25 was caused both by the disappearance of the pre-extinction large forms as well as the origination of smaller new species.

Another feature of ostracod morphological changes is that the percentage of the measured length/height (L/H) ratio beyond 2.75 in Assemblage II is significantly greater than in Assemblage I (Fig. 8). The maximum value of this ratio in Assemblage I is less than 3.5, while it is up to 5 for Assemblage II. Of course, it does not mean that all of the maximum values for each bed belonging to Assemblage II are larger than the values of Assemblage I, and some specimens from Beds 26 and 29, for instance, have values of less than 2 (Fig. 9, Table 2). In addition, changes in mean values of the L/H ratio are not remarkably large, but the increase in ratio follows a similar pattern to the maximum values (Fig. 9). For the minimum values of the L/H ratio, there are no significant changes between the two assemblages. The LOWESS curves indicated a weak growth trend across the turnover interval (Fig. 9B). The maximum, mean and minimum of the L/H ratio variations show the high occurrence of more elongated ostracods, and a number of the specimens have L/H ratios greater than 3 after the mass extinction. Furthermore, the trend in length/thickness ratio also shows a similar pattern to the L/H ratio.

6.2.2. Warming and decreased oxygen-dissolved concentrations

Temperature is one of the most important extrinsic factors for the growth and distribution of organisms (Hofmann and Todgham, 2010).

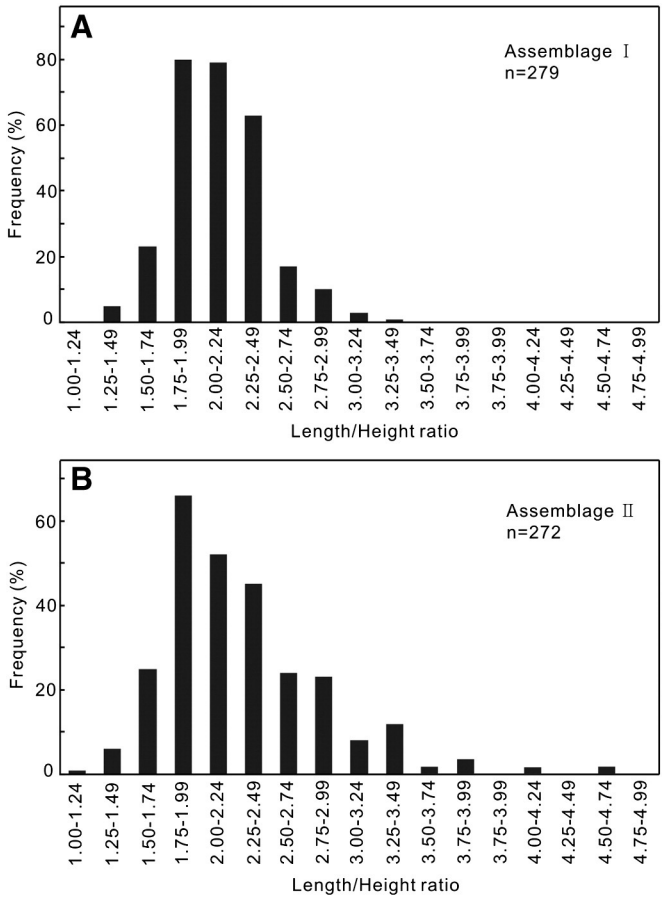

Fig. 8. Frequency of ostracod L/H ratio and the normal distribution curve of the two assemblages. (A) Assemblage I, showing tests having L/H ratios larger than 3 comprise 11.0% of all ostracods. (B) Assemblage II, showing ostracods having L/H ratios larger than 3 comprise 1.4% of all tests.

Generally, a suitable temperature rise that persists at normal levels benefits plants and animals, while rapid warming and high-level temperature can be lethal for most. A global mean rise of 5–10 °C probably caused severe heat stress for many marine and terrestrial organisms during the P–Tr mass extinction (Joachimski et al., 2012; Benton and Newell, 2014). Furthermore, there is growing evidence that lethal warming and anoxia were significant components of selective extinction during the P–Tr crisis (Berner et al., 2007; Payne and Clapham, 2012; H.J. Song et al., 2014) and only those organisms with high tolerance levels to warming and hypoxia could survive in the mid-water refuge zone in the marine environment (Beatty et al., 2008; H.J. Song et al., 2014), while Knoll et al. (2007) argued that hypercapnic stress from elevated *p*CO2 was the major driver of extinction selectivity. For lakes, the situation might have been worse, considering that the rate of temperature increase would have been greater on land than in the sea, as evidenced by findings of much-reduced bioturbation and the lack of body fossils of invertebrates in the Early Triassic of North China (Chu et al., 2015). Elevated temperature and reduced atmospheric oxygen pressure would have dramatically decreased the solubility of oxygen in lakes. In addition, Cao et al. (2008) recorded two distinct episodes of negative $\delta^{13}C_{org}$ shifts during the P–Tr transition from the SLA section, and the first of these suggest there was onset of environmental stress prior to the end-Permian mass extinction event, which is indicated by turnover in ostracod fauna. The negative $\delta^{13}C_{org}$ shift could be considered a sensitive response to the onset of the increasing *p*CO2 and the warming environment.

Modern long-term surveys, experimental data and simulations show that most ectothermic organisms mature at smaller body sizes when reared in warmer conditions, which is one of the most taxonomically widespread patterns in biology and is known as the "temperature-size rule" (Atkinson and Sibly, 1997; Daufresne et al., 2009). In addition, the study of the differences between ectothermic metazoans by environment and size indicates that warming-induced reductions in body size are greater in aquatic than terrestrial species, which suggests that oxygen is a major driver of temperature size responses in aquatic organisms (Forster et al., 2012). The warming and reduced oxygen-dissolved concentrations might have significantly led to the death of terrestrial invertebrates and the size decrease of terrestrial ostracods during the P–Tr crisis.

6.2.3. Enhanced input of terrestrial materials

Increased continental weathering is thought to have been the main contributor to the large and rapid global increase of seawater $^{87}Sr/^{86}Sr$ (~0.7070–0.7082) during the P–Tr mass extinction (Martin and MacDougall, 1995; Korte et al., 2003, 2004, 2006; Huang et al., 2008; Sedlacek et al., 2014; Song et al., 2015). Simultaneously, evidence for increased rates of erosion from terrestrial settings has been mentioned in studies of paleosols and lithological changes around the PTB (Retallack, 1995; Newell et al., 1999; Ward et al., 2000; Chakraborty and Sarkar, 2005; Sheldon, 2006). The increased rates of weathering and erosion directly led to enhanced input of terrestrial materials into rivers and lakes. As evidence for the direct effects of enhanced input at the time of the P–Tr mass extinction, Algeo and Twitchett (2010) noted clear indications of increased rates of terrestrial weathering near the P–Tr boundary in shallow marine settings worldwide, resulting from a significant increase in sediment fluxes to rivers and oceans.

The loss of land plant cover caused by wildfires is a well-known catalyst for terrestrial erosion and is accompanied by a strong influence on atmospheric composition (Benton and Newell, 2014). In recent studies, wildfires have been inferred from the abundance of charcoal, black carbon and carbon spherules in P–Tr event beds both in marine and terrestrial strata (Cao et al., 2008; S.Z. Shen et al., 2011; W.J. Shen et al., 2011). In addition, acid rain following the massive injection of volcanic gases into the atmosphere, associated with eruption of the Siberian Traps, would also have killed forests worldwide (Algeo and Twitchett, 2010; Sephton et al., 2015; Song et al., 2015). It is therefore possible

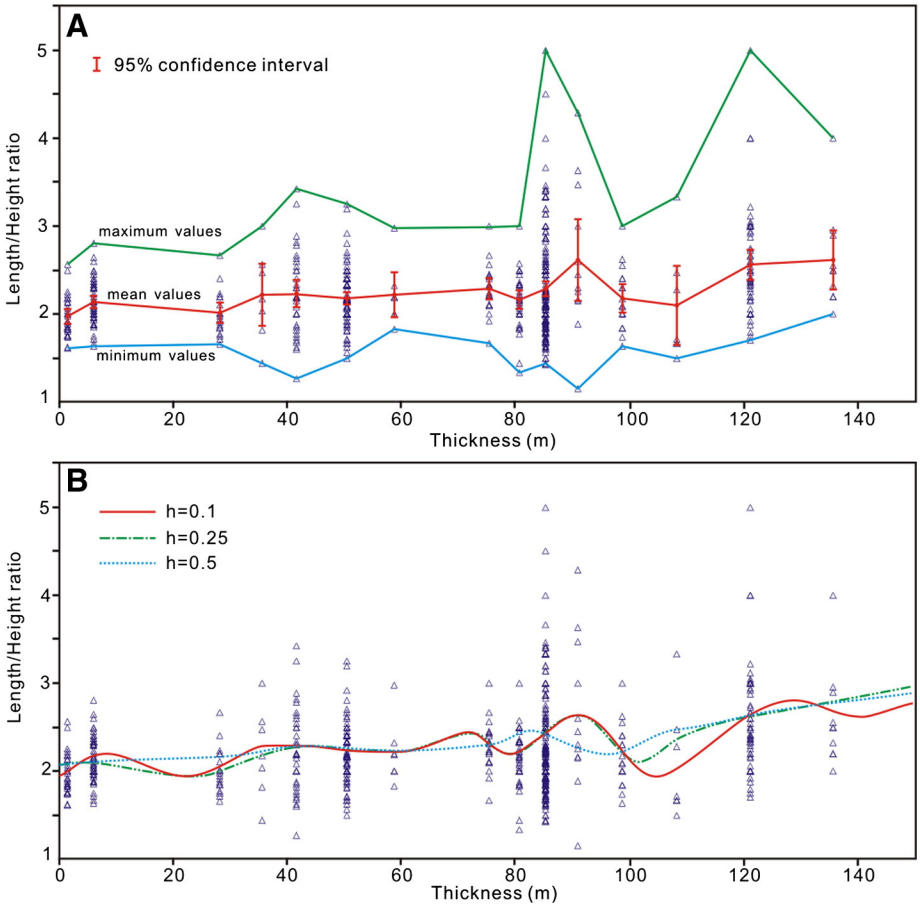

Fig. 9. L/H ratio distributions of ostracod tests through the Guodikeng Formation in the NLA section. (A) Plot detail of the L/H ratio for the different beds. The trend of the maximum and mean values shows the growing length/weight ratios, indicating the high occurrence of more elongate ostracods above Bed 24 in the NLA section. (B) LOWESS curves from the ostracod L/H ratio dataset, with *h* (window width) set at 0.1, 0.25 and 0.5, indicating a weak growth trend across the turnover interval.

that acid rain and wildfire might have caused a severe loss of plant cover and drove increasing sediment fluxes from land to freshwaters and to the sea.

These changes, accompanied by altered river morphology due to land plant extinctions, indicate a significantly enhanced input of terrestrial materials into rivers and lakes on land. Modern studies have suggested that the rapid sedimentation rate and discrete grain size distribution would have contributed to the reduction of ostracod body sizes and the absence of ostracods (Ruiz et al., 2013, and references therein). The increased influx of material likely placed pressure on ostracods by affecting their filter feeding efficiency and therefore hampering their growth.

6.3. The relationship between biotic crisis and size reduction

The P–Tr terrestrial biotic crisis is confirmed by the significant turnover and loss of life on land, as proposed by geologists and paleontologists from global-scale data. Plant diversity had declined substantially through the P–Tr mass extinction and even directly led to the Early Triassic "coal gap" (Veevers et al., 1994; Retallack

Table 2
The total number, maximum, minimum, mean, standard deviations, 95% confidence intervals (CI) of the mean and median length/height ratios of ostracod specimens in each bed at SLA section.

Bed number	Number of individuals	Maximum	Minimum	Mean	Standard deviation	95% CI of mean		Median
1	28	2.56	1.61	1.97	0.23	1.88	2.06	1.92
5	48	2.80	1.63	2.13	0.25	2.03	2.20	2.10
8	18	2.67	1.44	2.01	0.25	1.89	2.13	1.96
12	7	3.00	1.44	2.21	0.48	1.85	2.57	2.18
15	35	3.43	1.27	2.23	0.47	2.07	2.39	2.18
16	81	3.25	1.50	2.18	0.33	2.11	2.25	2.17
17	7	2.98	1.83	2.21	0.34	1.95	2.47	2.18
22	20	3.00	1.67	2.28	0.28	2.16	2.40	2.28
23	35	3.00	1.33	2.16	0.32	2.06	2.26	2.17
24	177	5.00	1.42	2.28	0.57	2.20	2.37	2.12
25	12	4.28	1.15	2.61	0.82	2.14	3.08	2.37
26	17	3.00	1.63	2.17	0.34	2.00	2.34	2.09
29	7	3.33	1.50	2.09	0.61	1.60	2.25	1.71
32	49	5.00	1.70	2.56	0.61	2.39	2.73	2.42
36	10	4.00	2.00	2.61	0.54	2.27	2.95	2.50

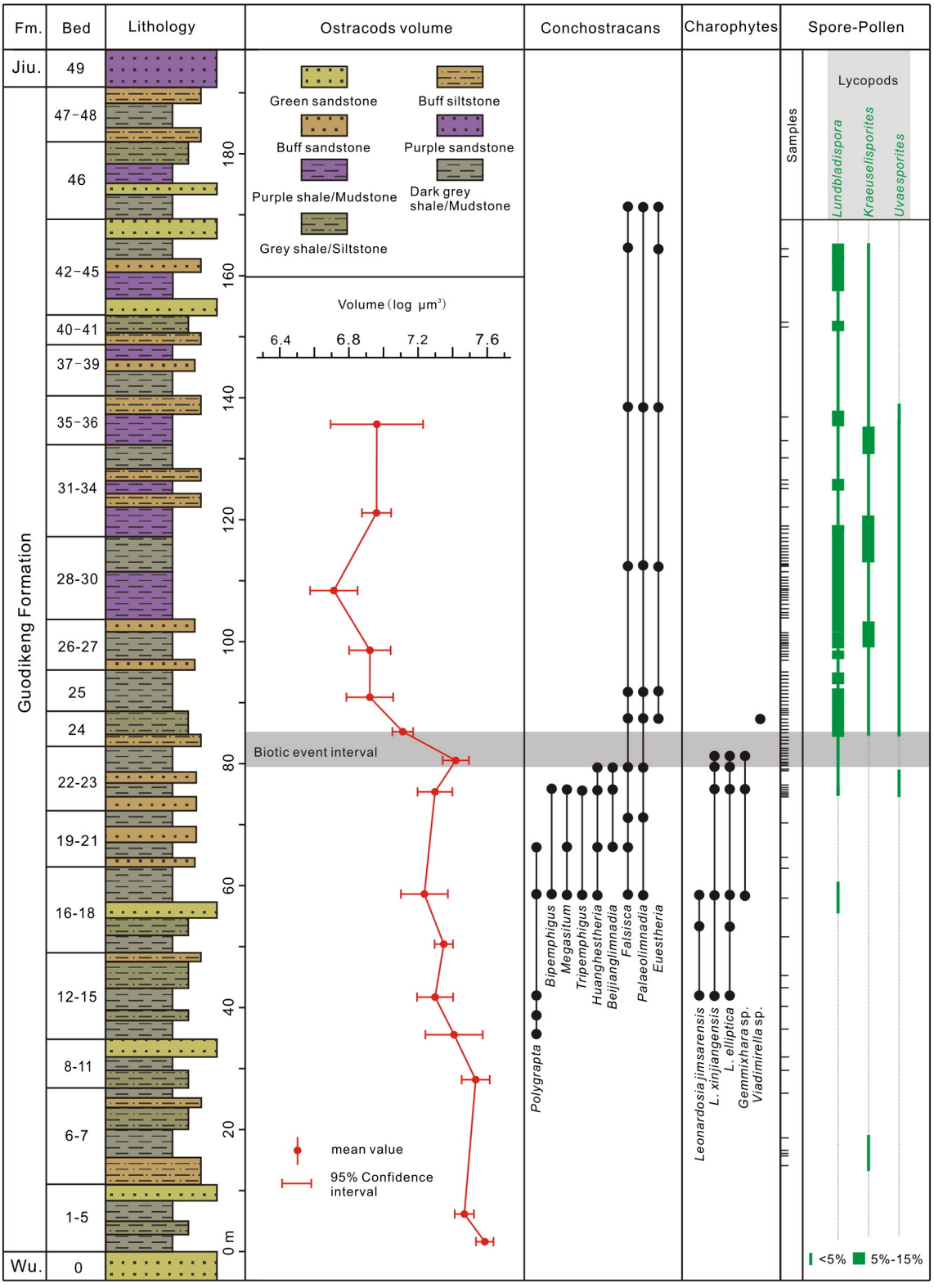

Fig. 10. Integrated stratigraphic sequences of the NLA section, showing the lithocolumn, size variation of the ostracod volumes, distributions of conchostracans, charophytes and lycopod spores at the section. Gray shaded area indicates the range of the biotic event interval. Abbreviations: Fm., Formation; Wu., Wutonggou Formation; Jiu., Jiucaiyuan Formation.

et al., 1996, 2011; Rees, 2002; Retallack, 2013). This conclusion is also supported by the evidence of global plant fossil records and high-resolution palynological data that show how the gymnosperm-dominated Permian floras were replaced by floras characterized by high abundances of lycopods associated with pteridosperms and conifers (Grauvogel-Stamm and Ash, 2005; Hermann et al., 2011). We also see this in the studied section; numerous lycopod spores appear above Bed 24, with a large abundance of the palynoflora *Kraeuselisporites*, *Lundbladispora*, and *Uvaesporites* (up to 30%, Fig. 10).

At present, ostracods and conchostracans were the most commonly studied materials among terrestrial invertebrates through the P–Tr transition, for example in regions of Russia (Kuchtinov, 1976; Mogutcheva and Krugovykh, 2009), Europe (Kukhtinov et al., 2008; Kozur and Weems, 2010), and China (Liu, 1987, 1994; Pang and Jin, 2004; Kozur and Weems, 2011). For ostracods, a high diversity of species of *Darwinula*, *Darwinuloides* and *Gerdalia* has been observed during the P–Tr transition in Russia (Kuchtinov, 1976; Mogutcheva and Krugovykh, 2009), Europe (Kukhtinov et al., 2008), and China (Pang and Jin, 2004). In our studied section, the most abundant genus is *Darwinula* (up to 90%), with high species diversity. There is a distinct turnover in the middle part of the Guodikeng Formation between Beds 23 and 24 (Fig. 2). For conchostracans, previous studies have shown that there is a significant extinction event horizon in the middle of the Hungtukun tuffs of the Tunguska Basin and the middle of the Guodikeng Formation in Northwest China (Liu, 1987, 1994; Kozur and Weems, 2011). The extinction event is also indicated by decreases at the genus level in the studied section. The most diverse conchostracan faunas were found in the Permian, characterized by eight genera below Bed 23, i.e., *Tripemphigus*, *Bipemphigus*, *Megasitum*, *Huanghestheria*, *Beijinalimnadia*, *Falsisca*, *Polygrapta*, *Palaeolimnadia*, and only two genera of *Falsisca* and several *Palaeolimnadia* species above the level of the extinction event in the NLA section (Fig. 10). In addition, typical later Permian examples of charophytes, *Leonardosia* and *Gemmixhara*, almost disappear at the same horizon (Fig. 10).

As discussed above, the size reduction of ostracods took place in the horizon where mass extinction of ostracods occurred. The extinction of the large ostracod species led directly to a significant decrease in the mean ostracod body size. Considering the rapid deposition rate, there is a coincidence between the horizons where ostracod size reduction occurred and the horizons of the main turnover of palynoflora and the extinction of conchostracans and charophytes; both occurred in an interval less than 6 m thick (Fig. 10), suggesting that the timing of the two events is related. In addition, the main causes of the size reduction of ostracods might have been warming, reduced dissolved-oxygen concentrations, and an increased input of terrestrial materials. As evidence for the effects of warming conditions, Sun et al. (2012) suggested that lethally hot temperatures were a major cause of the P–Tr biotic crisis, and Daufresne et al. (2009) described associations of warmer conditions with organisms of smaller body size, using long-term surveys, experimental data and published results. Moreover, the probably enhanced input of terrestrial material might be related to the mass extinction of land plants. The increased sedimentation rates and discrete grain size distribution would have contributed to the reduction of ostracod body sizes and the absence of ostracods (Ruiz et al., 2013).

In summary, the distinct ostracod size reduction associated with significant biotic turnover was limited to a short interval of less than 6 m in the middle part of the Guodikeng Formation. The size reduction might have been a response to selective mass extinction, both of which were driven by the same environmental conditions.

7. Conclusions

Quantitative analyses of one genus of terrestrial ostracods, *Darwinula*, from Northwest China reveal that ostracod test sizes decreased sharply through the terrestrial P–Tr mass extinction interval. The extinction of the large ostracods, accompanied by the arrival of small newcomers, led to a significant size reduction of the terrestrial ostracods and indicates evidence for the Lilliput effect in terrestrial aquatic invertebrates during the P–Tr biotic crisis. In addition, the strongest turnover of conchostracan faunas, charophytes, and the abundance of numerous "Triassic-type" lycopod spores occur in the same interval. The decrease in terrestrial ostracod sizes and the biotic crisis through the P–Tr interval may have been triggered by several defaunation events such as global warming, anoxia, and enhanced input due to acid rain and wildfire.

Acknowledgments

We thank Shucheng Xie for organizing the field trip. Yuan Tian, Liduan Zheng and Qing Ouyang helped with sampling from the studied section. We would like to acknowledge undergraduate volunteers Jun Zhu and Qingting Wu for their fossil finding and company in the field. This study was supported by the 973 Program (National Basic Research Program of China; 2011CB808800), the National Natural Science Foundation of China (41272372, 41302271, 41172312), the 111 Project (B08030), State Key Laboratory of Biogeology and Environmental Geology, China University of Geosciences, Wuhan (Program GBL11202, GBL11302), and the Fundamental Research Funds for the Central Universities (CUG1410491T01, CUGL140828).

Appendix A. Supplementary data

Supplementary data to this article can be found online at http://dx.doi.org/10.1016/j.palaeo.2015.06.003.

References

Algeo, T.J., Twitchett, R.J., 2010. Anomalous Early Triassic sediment fluxes due to elevated weathering rates and their biological consequences. Geology 38, 1023–1026.
Algeo, T.J., Chen, Z.Q., Fraiser, M.L., Twitchett, R.J., 2011. Terrestrial-marine teleconnections in the collapse and rebuilding of Early Triassic marine ecosystems. Palaeogeogr. Palaeoclimatol. Palaeoecol. 308, 1–11.
Atkinson, D., Sibly, R.M., 1997. Why are organisms usually bigger in colder environments? Making sense of a life history puzzle. Trends Ecol. Evol. 12, 235–239.
Beatty, T.W, Zonneveld, J.P., Henderson, C.M., 2008. Anomalously diverse Early Triassic ichnofossil assemblages in northwest Pangea: a case for a shallow-marine habitable zone. Geology 36, 771–774.
Benton, M.J., 1985. Mass extinction among non-marine tetrapods. Nature 316, 811–814.
Benton, M.J., 2003. When Life Nearly Died: The Greatest Mass Extinction of All Time. Thames & Hudson, London (336 pp.).
Benton, M.J., Newell, A.J., 2014. Impacts of global warming on Permo-Triassic terrestrial ecosystems. Gondwana Res. 25, 1308–1337.
Benton, M.J., Tverdokhlebov, V.P., Surkov, M., 2004. Ecosystem remodelling among vertebrates at the Permian–Triassic boundary in Russia. Nature 432, 97–100.
Berner, R.A., VandenBrooks, J.M., Ward, P.D., 2007. Oxygen and evolution. Science 316, 557–558.
Cao, C.Q., Wang, W., Liu, L.J., Shen, S.Z., Summons, R.E., 2008. Two episodes of ^{13}C-depletion in organic carbon in the latest Permian: evidence from the terrestrial sequences in northern Xinjiang, China. Earth Planet. Sci. Lett. 270, 251–257.
Chakraborty, T., Sarkar, S., 2005. Evidence of lacustrine sedimentation in the Upper Permian Bijori Formation, Satpura Gondwana basin: palaeogeographic and tectonic implications. J. Earth Syst. Sci. 114, 303–323.
Chen, Z.Q., Benton, M.J., 2012. The timing and pattern of biotic recovery following the end-Permian mass extinction. Nat. Geosci. 5, 375–383.
Chen, Z.Q., Kaiho, K., George, A.D., 2005. Survival strategies of brachiopod faunas from the end-Permian mass extinction. Palaeogeogr. Palaeoclimatol. Palaeoecol. 224, 232–269.
Cheng, Z.W., Wu, S.Z., Fang, X.S., 1997. The Permian–Triassic sequences in the southern margin of the Junggar Basin and the Turpan Basin, Xinjiang. Xinjiang Geol. 15, 155–173 (in Chinese with English abstract).
Chu, D.L., Tong, J.N., Song, H.J., Benton, M.J., Bottjer, D.J., Song, H.Y., Tian, L., 2015. Early Triassic wrinkle structures on land: stressed environments and oases for life. Sci. Rep. http://dx.doi.org/10.1038/srep10109.
Clapham, M.E., Payne, J.L., 2011. Acidification, anoxia, and extinction: a multiple logistic regression analysis of extinction selectivity during the Middle and Late Permian. Geology 39, 1059–1062.
Daufresne, M., Lengfellner, K., Sommer, U., 2009. Global warming benefits the small in aquatic ecosystems. Proc. Natl. Acad. Sci. U. S. A. 106, 12788–12793.
de Wit, M.J., Ghosh, J.G., de Villiers, S., Rakotosolofo, N., Alexander, J., Tripathi, A., Looy, C., 2002. Multiple organic carbon isotope reversals across the permo-triassic boundary of terrestrial Gondwana sequences: clues to extinction patterns and delayed ecosystem recovery. J. Geol. 110, 227–240.
Erwin, D.H., 1993. The Great Paleozoic Crisis: Life and Death in the Permian. Columbia University Press, New York (327 pp.).
Forster, J., Hirst, A.G., Atkinson, D., 2012. Warming-induced reductions in body size are greater in aquatic than terrestrial species. Proc. Natl. Acad. Sci. U. S. A. 109, 19310–19314.
Foster, C., Afonin, S., 2005. Abnormal pollen grains: an outcome of deteriorating atmospheric conditions around the Permian–Triassic boundary. J. Geol. Soc. 162, 653–659.
Fraiser, M.L., Bottjer, D.J., 2004. The non-actualistic Early Triassic gastropod fauna: a case study of the Lower Triassic SinbadLimestone member. Palaios 19, 259–275.
Girard, C., Renaud, S., 1996. Size variation in conodonts in response to the upper Kellwasser crisis (Upper Devonian of the Montagne Noire, France). C. R. Acad. Sci. III 323, 435–442.
Grasby, S., Beauchamp, B., Embry, A., Sanei, H., 2013. Recurrent Early Triassic ocean anoxia. Geology 41, 175–178.

Grauvogel-Stamm, L., Ash, S.R., 2005. Recovery of the Triassic land flora from the end-Permian life crisis. C. R. Palevol. 4, 593–608.
Hallam, A., Wignall, P.B., 1997. Mass Extinctions and Their Aftermath. Oxford University Press, Oxford (320 pp.).
Harries, P.J., Knorr, P.O., 2009. What does the 'Lilliput Effect' mean? Palaeogeography, Palaeoclimatology, Palaeoecology 284, 4–10.
Hayami, I., 1997. Size changes of bivalves and a hypothesis about the cause of mass extinction. Fossils 62, 24–36 (in Japanese).
He, W.H., Shi, G.R., Feng, Q.L., Campi, M.J., Gu, S.Z., Bu, J.J., Peng, Y.Q., Meng, Y.Y., 2007. Brachiopod miniaturization and its possible causes during the Permian–Triassic crisis in deep water environments, South China. Palaeogeogr. Palaeoclimatol. Palaeoecol. 252, 145–163.
He, W.H., Twitchett, R.J., Zhang, Y., Shi, G.R., Feng, Q.L., Yu, J.X., Wu, S.B., Peng, X.F., 2010. Controls on body size during the Late Permian mass extinction event. Geobiology 8, 391–402.
He, W.H., Shi, G.R., Twitchett, R.J., Zhang, Y., Zhang, K.X., Song, H.J., Yue, M.L., Wu, S.B., Wu, H.T., Yang, T.L., Xiao, Y.F., 2015. Late Permian marine ecosystem collapse began in deeper waters: evidence from brachiopod diversity and body size changes. Geobiology 13, 123–138.
Hermann, E., Hochuli, P.A., Bucher, H., Bruhwiler, T., Hautmann, M., Ware, D., Roohi, G., 2011. Terrestrial ecosystems on North Gondwana following the end-Permian mass extinction. Gondwana Res. 20, 630–637.
Hinojosa, J.L., Brown, S.T., Chen, J., DePaolo, D.J., Paytan, A., Shen, S.Z., Payne, J.L., 2012. Evidence for end-Permian ocean acidification from calcium isotopes in biogenic apatite. Geology 40, 743–746.
Hofmann, G.E., Todgham, A.E., 2010. Living in the now: physiological mechanisms to tolerate a rapidly changing environment. Annu. Rev. Physiol. 72, 127–145.
Hou, J.P., 2004. Two sporo-pollen assemblages of Guodikeng formation and discussion on the Permo-Triassic boundary in Junggar Basin, Xinjiang. Editorial Committee of Professional Papers of Stratigraphy and Palaeontology of Chinese Academy of Geological Sciences. Professional Papers of Stratigraphy and Palaeontology 28, pp. 177–204.
Huang, S.J., Qing, H.R., Huang, P.P., Hu, Z.W., Wang, Q.D., Zou, M.L., Liu, H.N., 2008. Evolution of strontium isotopic composition of seawater from Late Permian to Early Triassic based on study of marine carbonates, Zhongliang Mountain, Chongqing, China. Sci. China Ser. D Earth Sci. 51, 528–539.
Huttenlocker, A.K., 2014. Body size reductions in nonmammalian eutheriodont therapsids (Synapsida) during the end-Permian mass extinction. PLoS One 9, e87553.
Isozaki, Y., 1997. Permo–Triassic boundary superanoxia and stratified superocean: records from lost deep sea. Science 276, 235–238.
Jablonski, D., 1996. Body size and macroevolution. In: Jablonski, D., Erwin, D., Lipps, J. (Eds.), Evolutionary Paleobiology. Chicago Press, Chicago, pp. 256–289.
Jeffery, C.H., 2001. Heart urchins at the Cretaceous/Tertiary boundary: a tale of two clades. Paleobiology 27, 140–158.
Joachimski, M.M., Lai, X.L., Shen, S.Z., Jiang, H.S., Luo, G.M., Chen, B., Chen, J., Sun, Y.D., 2012. Climate warming in the latest Permian and the Permian–Triassic mass extinction. Geology 40, 195–198.
Kaljo, D., 1996. Diachronous recovery patterns in Early Silurian corals, graptolites and acritarchs. Geol. Soc. Lond., Spec. Publ. 102, 127–133.
Knoll, A.H., Bambach, R.K., Payne, J.L., Pruss, S., Fischer, W.W., 2007. Paleophysiology and end-Permian mass extinction. Earth Planet. Sci. Lett. 256, 295–313.
Korte, C., Kozur, H.W., Bruckschen, P., Veizer, J., 2003. Strontium isotope evolution of Late Permian and Triassic seawater. Geochim. Cosmochim. Acta 67, 47–62.
Korte, C., Kozur, H.W., Joachimski, M.M., Strauss, H., Veizer, J., Schwark, L., 2004. Carbon, sulfur, oxygen and strontium isotope records, organic geochemistry and biostratigraphy across the Permian/Triassic boundary in Abadeh, Iran. Int. J. Earth Sci. 93, 565–581.
Korte, C., Jasper, T., Kozur, H.W., Veizer, J., 2006. 87Sr/86Sr record of Permian seawater. Palaeogeogr. Palaeoclimatol. Palaeoecol. 240, 89–107.
Kozur, H.W., Mock, R., 1993. The importance of conchostracans for the correlation of continental and marine beds. In: Lucas, S.G., Morales, M. (Eds.), The nonmarine Triassic. New Mexico Museum of Natural History and Science Bulletin 3, pp. 261–266.
Kozur, H.W., Weems, R.E., 2010. The biostratigraphic importance of conchostracans in the continental Triassic of the northern hemisphere. Geol. Soc. Lond., Spec. Publ. 334, 315–417.
Kozur, H.W., Weems, R.E., 2011. Detailed correlation and age of continental late Changhsingian and earliest Triassic beds: implications for the role of the Siberian Trap in the Permian–Triassic biotic crisis. Palaeogeogr. Palaeoclimatol. Palaeoecol. 308, 22–40.
Krull, E.S., Retallack, G.J., 2000. $\delta^{13}C$ depth profiles from paleosols across the Permian–Triassic boundary: evidence for methane release. Geol. Soc. Am. Bull. 112, 1459–1472.
Kuchtinov, D.A., 1976. Biostratigraphy of the Triassic Deposits of the Pre-Caspian Syneclise on the Base of Ostracods. Nedra, Moscow (99 pp., in Russian).
Kukhtinov, D.A., Lozovsky, V.R., Afonin, S.A., Voronkova, E.A., 2008. Non-marine ostracods of the Permian–Triassic transition from sections of the East European platform: stratigraphy and palaeogeography of late- and post-Hercynian basins in the Southern Alps, Tuscany and Sardinia (Italy). Boll. Soc. Geol. Ital. 127, 717–726.
Liu, S.W., 1987. Some Permian–Triassic conchostracans and their significance of geological age from the middle area of Tianshan Mountains. Prof. Pap. Stratigr. Palaeontol. 18, 92–116.
Liu, S.W., 1994. The non-marine Permian–Triassic boundary and Triassic conchostracan fossils in China. Albertiana 13, 12–24.
MacLeod, K.G., Smith, R.M., Koch, P.L., Ward, P.D., 2000. Timing of mammal-like reptile extinctions across the Permian–Triassic boundary in South Africa. Geology 28, 227–230.
Martin, E.E., MacDougall, J.D., 1995. Sr and Nd isotopes at the Permian/Triassic boundary: a record of climate change. Chem. Geol. 125, 73–100.
McGowan, A.J., Smith, A.B., Taylor, P.D., 2009. Faunal diversity, heterogeneity and body size in the Early Triassic: testing post-extinction paradigms in the Virgin Limestone of Utah, USA. Aust. J. Earth Sci. 56, 859–872.
Metcalfe, I., Foster, C.B., Afonin, S.A., Nicoll, R.S., Mundil, R., Wang, X.F., Lucas, S.G., 2009. Stratigraphy, biostratigraphy and C-isotopes of the Permian–Triassic non-marine sequence at Dalongkou and Lucaogou, Xinjiang Province, China. J. Asian Earth Sci. 36, 503–520.
Metcalfe, I., Crowley, J.L., Nicoll, R.S., Schmitz, M., 2015. High-precision U–Pb CA-TIMS calibration of Middle Permian to Lower Triassic sequences, mass extinction and extreme climate-change in eastern Australian Gondwana. Gondwana Res. http://dx.doi.org/10.1111/brv.12161.
Mogutcheva, N.K., Krugovykh, V.V., 2009. New data on the stratigraphic chart for Triassic deposits in the Tunguska syneclise and Kuznetsk basin. Stratigr. Geol. Correl. 17, 510–518.
Morante, R., 1996. Permian and early Triassic isotopic records of carbon and strontium in Australia and a scenario of events about the Permian–Triassic boundary. Hist. Biol. 11, 289–310.
Mutter, R.J., Neuman, A.G., 2009. Recovery from the end-Permian extinction event: evidence from "Lilliput Listracanthus". Palaeogeogr. Palaeoclimatol. Palaeoecol. 284, 22–28.
Newell, A.J., Tverdokhlebov, V.P., Benton, M.J., 1999. Interplay of tectonics and climate on a transverse fluvial system, Upper Permian, Southern Uralian Foreland Basin, Russia. Sediment. Geol. 127, 11–29.
Pang, Q.Q., 1993. The nonmarine Triassic and Ostracoda in northern China. N. M. Mus. Nat. Hist. Sci. Bull. 3, 383–392.
Pang, Q.Q., Jin, X.C., 2004. Ostrocoda in the Guodikeng formation and continental Permo–Triassic boundary of Dalongkou section, Jimsar, Xinjiang. Editorial Committee of Professional Papers of Stratigraphy and Palaeontology of Chinese Academy of Geological Sciences. Professional Papers of Stratigraphy and Palaeontology 28, pp. 205–246.
Payne, J.L., 2005. Evolutionary dynamics of gastropod size across the end-Permian extinction and through the Triassic recovery interval. Paleobiology 31, 269–290.
Payne, J.L., Clapham, M.E., 2012. End-Permian mass extinction in the oceans: an ancient analog for the twenty-first century? Annu. Rev. Earth Planet. Sci. 40, 89–111.
Rees, P.M., 2002. Land-plant diversity and the end-Permian mass extinction. Geology 30, 827–830.
Renaud, S., Girard, C., 1999. Strategies of survival during extreme environmental perturbations: evolution of conodonts in response to the Kellwasser crisis (Upper Devonian). Palaeogeogr. Palaeoclimatol. Palaeoecol. 146, 19–32.
Retallack, G.J., 1995. Permian–Triassic life crisis on land. Science 267, 77–80.
Retallack, G.J., 2013. Permian and Triassic greenhouse crises. Gondwana Res. 24, 90–103.
Retallack, G.J., Krull, E.S., 2006. Carbon isotopic evidence for terminal-Permian methane outbursts and their role in extinctions of animals, plants, coral reefs, and peat swamps. Geol. Soc. Am. Spec. Pap. 399, 249–268.
Retallack, G.J., Veevers, J.J., Morante, R., 1996. Global coal gap between Permian–Triassic extinction and Middle Triassic recovery of peat-forming plants. Geol. Soc. Am. Bull. 108, 195–207.
Retallack, G.J., Smith, R.M., Ward, P.D., 2003. Vertebrate extinction across Permian–Triassic boundary in Karoo Basin, South Africa. Geol. Soc. Am. Bull. 115, 1133–1152.
Retallack, G.J., Sheldon, N.D., Carr, P.F., Fanning, M., Thompson, C.A., Williams, M.L., Jones, B.G., Hutton, A., 2011. Multiple Early Triassic greenhouse crises impeded recovery from Late Permian mass extinction. Palaeogeogr. Palaeoclimatol. Palaeoecol. 308, 233–251.
Romano, C., Koot, M.B., Kogan, I., Brayard, A., Minikh, A.V., Brinkmann, W., Bucher, H., Kriwet, J., 2015. Permian–Triassic Osteichthyes (bony fihes): diversity dynamics and body size evolution. Biol. Rev. http://dx.doi.org/10.1111/brv.12161.
Ruiz, F., Abad, M., Bodergat, A., Carbonel, P., Rodríguez-Lázaro, J., González-Regalado, M.L., Toscano, A., García, E., Prenda, J., 2013. Freshwater ostracods as environmental tracers. Int. J. Environ. Sci. Technol. 10, 1115–1128.
Sedlacek, A.R., Saltzman, M.R., Algeo, T.J., Horacek, M., Brandner, R., Foland, K., Denniston, R.F., 2014. 87Sr/86Sr stratigraphy from the Early Triassic of Zal, Iran: linking temperature to weathering rates and the tempo of ecosystem recovery. Geology 42, 779–782.
Sephton, M.A., Jiao, D., Engel, M.H., Looy, C.V., Visscher, H., 2015. Terrestrial acidification during the end-Permian biosphere crisis? Geology 43, 159–162.
Sheldon, N.D., 2006. Abrupt chemical weathering increase across the Permian–Triassic boundary. Palaeogeogr. Palaeoclimatol. Palaeoecol. 231, 315–321.
Shen, S.Z., Crowley, J.L., Wang, Y., Bowring, S.A., Erwin, D.H., Sadler, P.M., Cao, C.Q., Rothman, D.H., Henderson, C.M., Ramezani, J., Zhang, H., Shen, Y., Wang, X.D., Wang, W., Mu, L., Li, W.Z., Tang, Y.G., Liu, X.L., Liu, L.J., Zeng, Y., Jiang, Y.F., Jin, Y.G., 2011a. Calibrating the end-Permian mass extinction. Science 334, 1367–1372.
Shen, W.J., Sun, Y.G., Lin, Y.T., Liu, D.H., Chai, P.X., 2011b. Evidence for wildfire in the Meishan section and implications for Permian–Triassic events. Geochim. Cosmochim. Acta 75, 1992–2006.
Sohn, I.G., 1961. Techniques for preparation and study of fossil ostracodes. Q64–Q70. In: Moore, R.C. (Ed.), Treatise of Invertebrate Paleontology. Part Q, Arthropoda 3. Geological Society of America, Boulder, and University of Kansas Press, Lawrence (442 pp.).
Song, H.J., Wignall, P.B., Chen, Z.Q., Tong, J.N., Bond, D.P., Lai, X.L., Zhao, X.M., Jiang, H.S., Yan, C.B., Niu, Z.J., Chen, J., Yang, H., Wang, Y.B., 2011a. Recovery tempo and pattern of marine ecosystems after the end-Permian mass extinction. Geology 39, 739–742.
Song, H.J., Tong, J.N., Chen, Z.Q., 2011b. Evolutionary dynamics of the Permian–Triassic foraminifer size: evidence for Lilliput effect in the end-Permian mass extinction and its aftermath. Palaeogeogr. Palaeoclimatol. Palaeoecol. 308, 98–110.
Song, H.J., Wignall, P.B., Tong, J.N., Bond, D.P., Song, H.Y., Lai, X.L., Zhang, K.X., Wang, H.M., Chen, Y.L., 2012. Geochemical evidence from bio-apatite for multiple oceanic anoxic

events during Permian–Triassic transition and the link with end-Permian extinction and recovery. Earth Planet. Sci. Lett. 353, 12–21.
Song, H.J., Wignall, P.B., Tong, J.N., Yin, H.F., 2013. Two pulses of extinction during the Permian–Triassic crisis. Nat. Geosci. 6, 52–56.
Song, H.J., Wignall, P.B., Chu, D.L., Tong, J.N., Sun, Y.D., Song, H.Y., He, W.H., Tian, L., 2014a. Anoxia/high temperature double whammy during the Permian–Triassic marine crisis and its aftermath. Sci. Rep. 4, e4132.
Song, H.Y., Tong, J.N., Algeo, T.J., Song, H.J., Qiu, H.O., Zhu, Y.Y., Tian, L., Bates, S., Lyons, T.W., Luo, G.M., Kump, L.R., 2014b. Early Triassic seawater sulfate drawdown. Geochim. Cosmochim. Acta 128, 95–113.
Song, H.J., Wignall, P.B., Tong, J.N., Song, H.Y., Chen, J., Chu, D.L., Tian, L., Luo, M., Zong, K.Q., Chen, Y.L., Lai, X.L., Zhang, K.X., Wang, H.M., 2015. Integrated Sr isotope variations and global environmental changes through the Late Permian to early Late Triassic. Earth Planet. Sci. Lett. http://dx.doi.org/10.1016/j.epsl.2015.05.035.
Sun, Y.D., Joachimski, M.M., Wignall, P.B., Yan, C.B., Chen, Y.L., Jiang, H.S., Wang, L.N., Lai, X.L., 2012. Lethally hot temperatures during the early Triassic greenhouse. Science 338, 366–370.
Tian, L., Tong, J.N., Algeo, T.J., Song, H.J., Song, H.Y., Chu, D.L., Shi, L., Bottjer, D.J., 2014. Reconstruction of Early Triassic ocean redox conditions based on framboidal pyrite from the Nanpanjiang Basin, South China. Palaeogeogr. Palaeoclimatol. Palaeoecol. 412, 68–79.
Tverdokhlebov, V.P., Tverdokhlebova, G.I., Surkov, M.V., Benton, M.J., 2002. Tetrapod localities from the Triassic of the SE of European Russia. Earth Sci. Rev. 60, 1–66.
Twitchett, R.J., 2007. The Lilliput effect in the aftermath of the end-Permian extinction event. Palaeogeogr. Palaeoclimatol. Palaeoecol. 252, 132–144.
Twitchett, R.J., Looy, C.V., Morante, R., Visscher, H., Wignall, P.B., 2001. Rapid and synchronous collapse of marine and terrestrial ecosystems during the end-Permian biotic crisis. Geology 29, 351–354.
Twitchett, R.J., Feinberg, J.M., O'Connor, D.D., Alvarez, W., McCollum, L.B., 2005. Early Triassic ophiuroids: their paleoecology, taphonomy, and distribution. Palaios 20, 213–223.
Urbanek, A., 1993. Biotic crises in the history of Upper Silurian graptoloids: a palaeobiological model. Hist. Biol. 7, 29–50.
Veevers, J.J., Conaghan, P.J., Shaw, S.E., 1994. Turning point in Pangean environmental history at the Permian/Triassic (P/Tr) boundary. In: Klein, G.D. (Ed.), Pangea: paleoclimate, tectonics, and sedimentation during accretion, zenith, and breakup of a supercontinent. Geological Society of America Special Paper 288, pp. 187–196.
Wang, S.Q., 1978. Later Permian and Early Triassic ostracods of Western Guizhou and Northestern Yunnan. Acta Palaeontol. Sin. 3, 277–318.
Ward, P.D., Montgomery, D.R., Smith, R., 2000. Altered river morphology in South Africa related to the Permian–Triassic extinction. Science 289, 1740–1743.
Wignall, P.B., Twitchett, R.J., 1996. Oceanic anoxia and the end Permian mass extinction. Science 272, 1155–1158.
Yu, J.X., Broutin, J., Chen, Z.Q., Shi, X., Li, H., Chu, D.L., Huang, Q.S., 2015. Vegetation changeover across the Permian–Triassic Boundary in Southwest China. Extinction, survival, recovery and palaeoclimate: a critical review. Earth Sci. Rev. http://dx.doi.org/10.1016/j.earscirev.2015.04.005.